

Article

Purification and Phase Evolution Mechanism of Titanium Oxycarbide (TiC_xO_y) Produced by the Thermal Reduction of Ilmenite

Chunlin He ^{1,2,*}, Chunhui Zheng ¹, Wei Dai ¹, Toyohisa Fujita ^{1,2} , Jian Zhao ¹, Shaojian Ma ^{1,2}, Xinsheng Li ^{1,2}, Yuezhou Wei ^{1,2,3} , Jinlin Yang ^{1,2} and Zongwu Wei ^{1,2}

- ¹ School of Resources, Environment and Materials, Guangxi University, Nanning 530004, China; zhengchunhuiya@126.com (C.Z.); daiweianhui@126.com (W.D.); fujitatoyohisa@gxu.edu.cn (T.F.); ZJ19780823@163.com (J.Z.); msj@gxu.edu.cn (S.M.); xinshengli@gxu.edu.cn (X.L.); yzwei@gxu.edu.cn (Y.W.); jlyang523@126.com (J.Y.); fangshen@gxu.edu.cn (Z.W.)
- ² Guangxi Key Laboratory of Processing for Non-ferrous Metal and Featured Materials, Nanning 530004, China
- ³ School of Nuclear Science and Engineering, Shanghai Jiao Tong University, Shanghai 200240, China
- * Correspondence: helink@gxu.edu.cn or helink1900@126.com

Abstract: The phase evolution mechanism and purification of titanium oxycarbide (TiC_xO_y) synthesized via the carbothermal reduction of ilmenite are investigated. The reaction process and products of the performed carbothermal reduction are analyzed by means of X-ray diffraction (XRD), scanning electron microscopy-energy disperse spectroscopy (SEM-EDS), X-ray photoelectric spectroscopy (XPS) and enthalpy, entropy and heat capacity (HSC) thermodynamic software. According to the shapes of Ti 2p_{3/2} and Ti 2p_{1/2} peaks in XPS spectra, together with the XRD analyses, the reduction products of TiO, TiC_xO_y or TiC can be judged. The phase evolution mechanism involves FeTi_2O_5 , Ti_2O_3 , Fe, TiO, TiC_xO_y and TiC under enhancing the content of carbon. The phase evolution law can be written as $\text{FeTiO}_3 \rightarrow \text{FeTi}_2\text{O}_5 \rightarrow \text{Ti}_2\text{O}_3 + \text{Fe} \rightarrow \text{TiO} + \text{Fe} \rightarrow \text{TiC}_x\text{O}_y + \text{Fe}$. Due to the incomplete reduction state of TiC_xO_y , the ΔG^0 of TiC_xO_y is detected between TiC and TiO. TiC_xO_y could be attained under reduction conditions of Ti:C, 1:3–1:4 in argon atmosphere at 1550 °C after 2 h. Grinding, flotation and magnetic separation processes displayed that C, TiC_xO_y and Fe are not dissociated until the particle size of $-38 \mu\text{m}$. TiC_xO_y and Fe can be separated by an iron-bath in a high temperature. 95.56% TiC_xO_y can be obtained, and resistance of TiC_xO_y is less than 0.05 Ω .

Keywords: ilmenite; carbothermal reduction; titanium oxycarbide; titanium metal



Citation: He, C.; Zheng, C.; Dai, W.; Fujita, T.; Zhao, J.; Ma, S.; Li, X.; Wei, Y.; Yang, J.; Wei, Z. Purification and Phase Evolution Mechanism of Titanium Oxycarbide (TiC_xO_y) Produced by the Thermal Reduction of Ilmenite. *Minerals* **2021**, *11*, 104. <https://doi.org/10.3390/min11020104>

Received: 12 November 2020
Accepted: 15 January 2021
Published: 21 January 2021

Publisher's Note: MDPI stays neutral with regard to jurisdictional claims in published maps and institutional affiliations.



Copyright: © 2021 by the authors. Licensee MDPI, Basel, Switzerland. This article is an open access article distributed under the terms and conditions of the Creative Commons Attribution (CC BY) license (<https://creativecommons.org/licenses/by/4.0/>).

1. Introduction

Titanium and its alloys are important lightweight, structural and new functional materials [1,2] due to their excellent physical and chemical properties such as low density, high strength, high temperature stability and excellent corrosion resistance. Titanium is widely used in the aerospace, military and chemical industries, shipping, construction, sporting equipment, medical tools, biomedical and other civil fields; thus, it is known as the “The space of metal” and “Marine metal” [3–9]. Titanium minerals include ilmenite, titanomagnetite, vanadium titanomagnetite and rutile [10,11]. At present, Kroll (magnesium thermal reduction) [12,13], Hunter (sodium thermal reduction) [14], FFC (Cambridge process) [15–18], OS (Ono Suzuki) [19], EMR/MSE (Electronically Mediated Reaction/Molten Salt Electrolysis) [20,21], PRP (preformed reduction process) [22] and USTB (University of Science and Technology Beijing) methodology [23–25] are the principal methods to prepare titanium metal. Among them, Kroll and Hunter methods have been industrialized for a long time. However, Kroll has the disadvantages of a complex process, large energy consumption, long production period, high cost and great environmental pollution, which greatly restricted the development and utilization of titanium. Hunter is a low-cost method for the production, transportation and storage of the reductant; however, it suffers from

the disadvantages of the Hunter process with low recovery of Ti, poor castability of sponge titanium and high content of chlorine. Therefore, the whole cost of the Hunter method is relatively higher than that of the Kroll method, and its industrial applications are limited.

A new electrolytic reduction procedure (USTB) was developed by Zhu Hongmin's research team based on the refining of titanium by using Ti oxycarbides as the anode in 2005 [23–26]. This methodology significantly overcomes the aforementioned shortcomings such as exclusively improved efficiency, reduction of impurities and amelioration of the electrolytic quality of metallic titanium [27]. One of the key factors of the method is to produce highly qualified titanium oxycarbide (TiC_xO_y , $x + y = 1$) or $\text{TiC}_x\text{O}_{1-x}$ ($0 < x < 1$). In the USTB, process the anode material is prepared via carbothermal reduction of pure TiO_2 or from a sintering mixture of pure TiO_2 and TiC [23,24,28–31]. Therefore, if titanium minerals could be directly reduced by carbothermal treatment to produce highly pure TiC_xO_y in the titanium enterprise and simultaneously carry out USTB process towards titanium, the total cost of the metal production would be significantly reduced, and the competitiveness of the enterprise can be significantly improved. TiC_xO_y is an intermediate during carbothermal reduction of ilmenite concentrates or ilmenite slag [32–34] in the presence of a certain amount of reductant and under a suitable temperature. Over the past decades, many works have been conducted on the mechanism and kinetics of the reduction of ilmenite, TiO_2 and titanium slag [35–43]. Most people focus on carbothermal reduction of ilmenite or titanium slag to prepare TiO_2 or TiC, but they have not been concerned about the usage of TiC_xO_y in the production of metallic Ti. In addition, most of ilmenite is used to prepare TiO_2 pigment by chloride process and sulphate process [10,44,45]. In the market, however, the price of titanium metal is three to five times more expensive than TiO_2 pigment. In order to better enhance the value of ilmenite, preparation of TiC_xO_y from ilmenite is suggested for titanium enterprise.

Therefore, in our work, we focus on carbothermal reduction of ilmenite to prepare TiC_xO_y . Especially, the phase evolution mechanism was investigated by combination of thermodynamic analysis and the phase of reduction product. The ΔG^θ of TiC_xO_y can be inferred from the reduction process of TiO or Ti_2O_3 ($\text{TiO}/\text{Ti}_2\text{O}_3 \rightarrow \text{TiC}_x\text{O}_y \rightarrow \text{TiC}$) through thermodynamic analysis. In addition, TiC is isomorphous with TiO. It is easy to misjudge the phase of reduction product only by XRD patterns, which were used widely [23–43]. Because titanium in TiC and TiO shows distinct chemical affinity towards oxygen and carbon, the XPS was carried out through studying the Ti 2p binding energy of TiO and TiC to further clarify the phase of the reduction product and to determine the reliability of TiC_xO_y in the reduction product. And then general parameters of carbon's ratio, reduction temperature and time are also studied. Thereafter, purification of TiC_xO_y is carried out by means of magnetic separation, acid leaching and iron-bath. This research can provide high-quality and front-end raw materials for the USTB process to furnish electrolysis of titanium from ilmenite, as an inexpensive substrate. This report provides basic parameters to reduce the cost of making titanium metal and improves the competitiveness of the existing enterprises.

2. Materials and Methods

The ilmenite concentrates were taken from Jin Mao Titanium Industry Company in Guangxi, China. Pure grade graphite powder was used as the reducing agent. The X-ray diffractometer pattern (XRD) and energy dispersive spectrometer (EDS) of the ilmenite concentrate are shown in Figure 1a,b, respectively. The analysis results of X-ray fluorescence spectra (Shimadzu XRF-1800, Shimadzu Corporation, Kyoto, Japan; current 140 mA, voltage 60 kV; the standard used for XRF analysis is JY/T 016-1995) are described in Table 1. According to the XRD and EDS results in Figure 1, the main phase of the raw ore is ilmenite (FeTiO_3). In addition, XRF findings showed that the contents of TiO_2 and Fe_2O_3 in the sample are 44.18 and 45.74 wt %, respectively, and the main impurities are SiO_2 , MgO, Al_2O_3 and CaO.

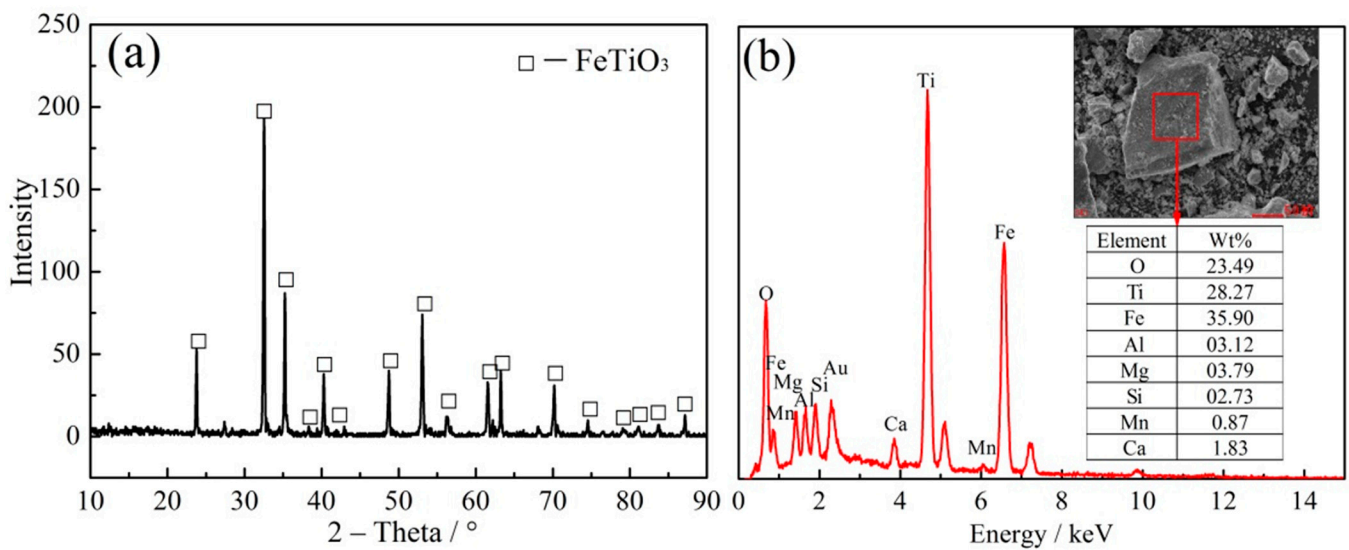


Figure 1. (a) XRD pattern and (b) EDS analysis of the ilmenite sample.

Table 1. The main chemical composition of ilmenite concentrate (wt %).

Chemical Composition	TFe	Fe ₂ O ₃	SiO ₂	TiO ₂	MnO	MgO	Al ₂ O ₃	CaO
Content	21.3	45.74	3.46	44.18	1.06	2.14	1.07	1.07

Figure 2 depicts a flow diagram for the whole process. The mass of ilmenite concentrate was fixed at 10 g and the content of carbon was calculated according to the molar ratio of Ti:C, as calculated based on the mass of graphite powder. The graphite and ilmenite concentrate were ground in an agate mortar until mixed evenly and then, the sample was pressed by a tablet machine with the pressure of 8 MPa for 15 min. The diameter and height of the block sample after pressing were 20 and 10 mm, respectively. Then, the pressed sample was placed in a tubular furnace and reduced under an argon atmosphere (Sections 3.1 and 3.2). After that, ball grinding along with flotation, magnetic separation, acid dissolution and separation by iron-bath were consecutively carried out (Section 3.4).

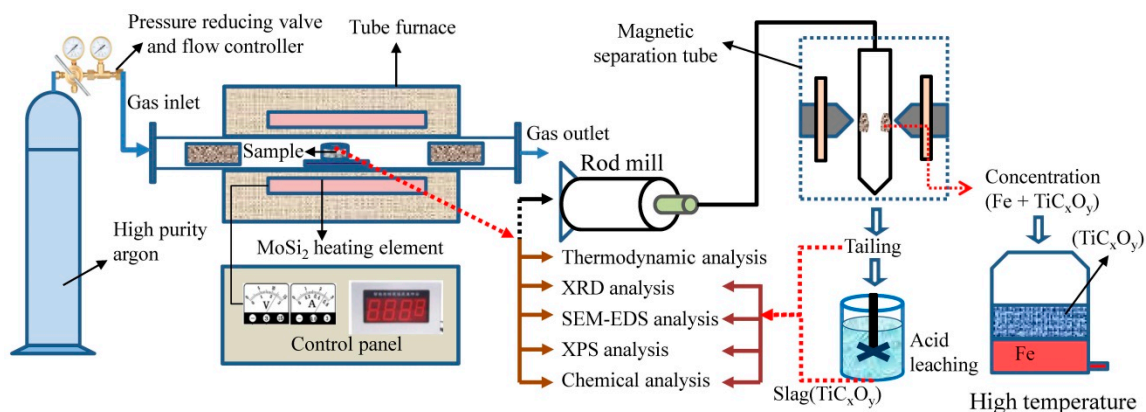


Figure 2. Flow diagram of the whole process.

XRD (Rigaku D/MAX 2500V, Japan; Cu-K α source, maximum voltage/current, 60 kV and 300 mA) was used to identify the phases of sample under the scanning speed of 10 $^\circ$ /min and scanning angle of 10–90 $^\circ$ (Sections 3.1 and 3.2). The SEM and EDs of Phenom company (Phenom Pro 800-07334, Phenom-World Corporation, Eindhoven, Noord-Brabant, Netherlands) was used to investigate the microstructure of product (Sections 3.1 and 3.4).

An X-ray photoelectron spectrometer (XPS, Thermo ESCALAB 250XI+, Thermo Fisher Scientific Corporation, Waltham, MA, USA) was applied to analyze Ti 2p states of TiO and TiC (Section 3.1.2), and then reveal distinct chemical affinity of Ti towards oxygen and carbon, and clarify the phase of the reduction product and determine the reliability of TiC_xO_y in the reduction product.

The possible reactions of ilmenite during carbon thermal reduction treatment were analyzed from the thermodynamic points of view. The reaction conditions were judged by calculating the changes of Gibbs function under the standard molar reactions (ΔG^θ) at different temperatures by HSC Chemistry 6.0 [46,47] combined with the phase of carbothermic reduction (Section 3.3). Then the phase evolution mechanism was investigated by combination of thermodynamic analysis and the phase of reduction product.

3. Results and Discussion

3.1. Effect of Carbon Molar Ratio on the Carbothermal Reduction

3.1.1. Phase Analysis of the Reduced Products

The carbon molar ratio (Ti:C) in carbon thermal reduction was 1:0.25–1:7 (the mass fraction of carbon was 10.51–35.77%), as shown in Table 2. The reduction temperature was 1550 °C at the reduction time of 4 h. The XRD patterns of the reduction products under different carbon ratios are shown in Figure 3a–e. XRD patterns of the reduction product containing TiO, TiC and TiC_xO_y (samples 7–15 with the 2θ in the range of 41.7–42.5°) are shown in Figure 3f.

Table 2. Titanium and carbon ratio.

	1	2	3	4	5	6	7	8	9	10
n(Ti):n(C)	1:0.25	1:0.5	1:0.75	1:1	1:1.25	1:1.5	1:1.75	1:2	1:2.5	1:3
Mass/%	10.51	11.81	13.07	14.29	15.47	16.63	17.75	18.84	20.94	22.92
	11	12	13	14	15					
n(Ti):n(C)	1:3.5	1:4	1:5	1:6	1:7					
Mass/%	24.81	26.61	29.95	32.99	35.77					

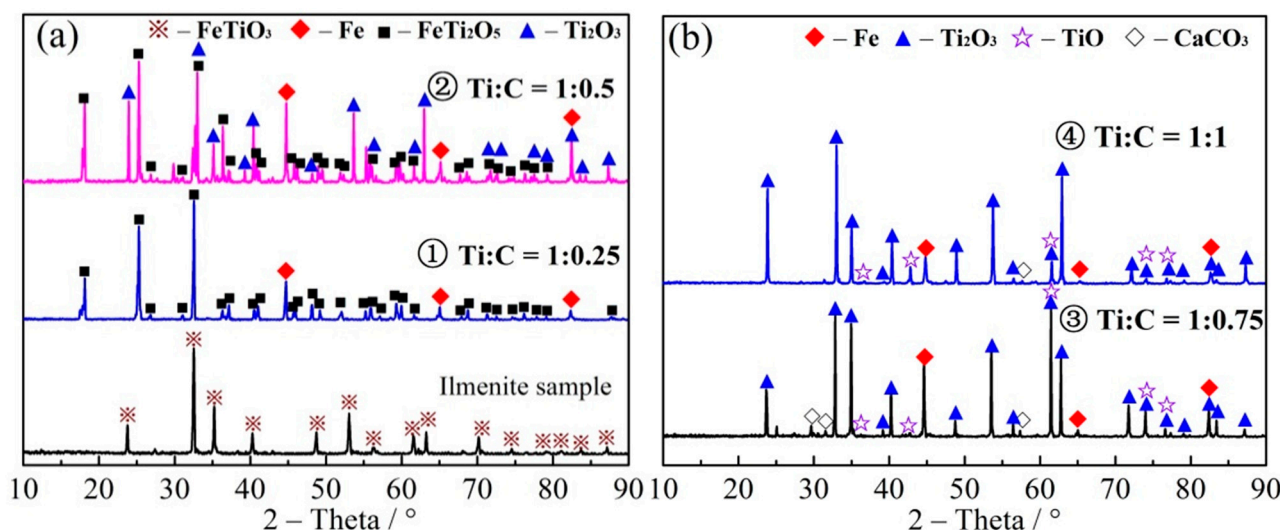


Figure 3. Cont.

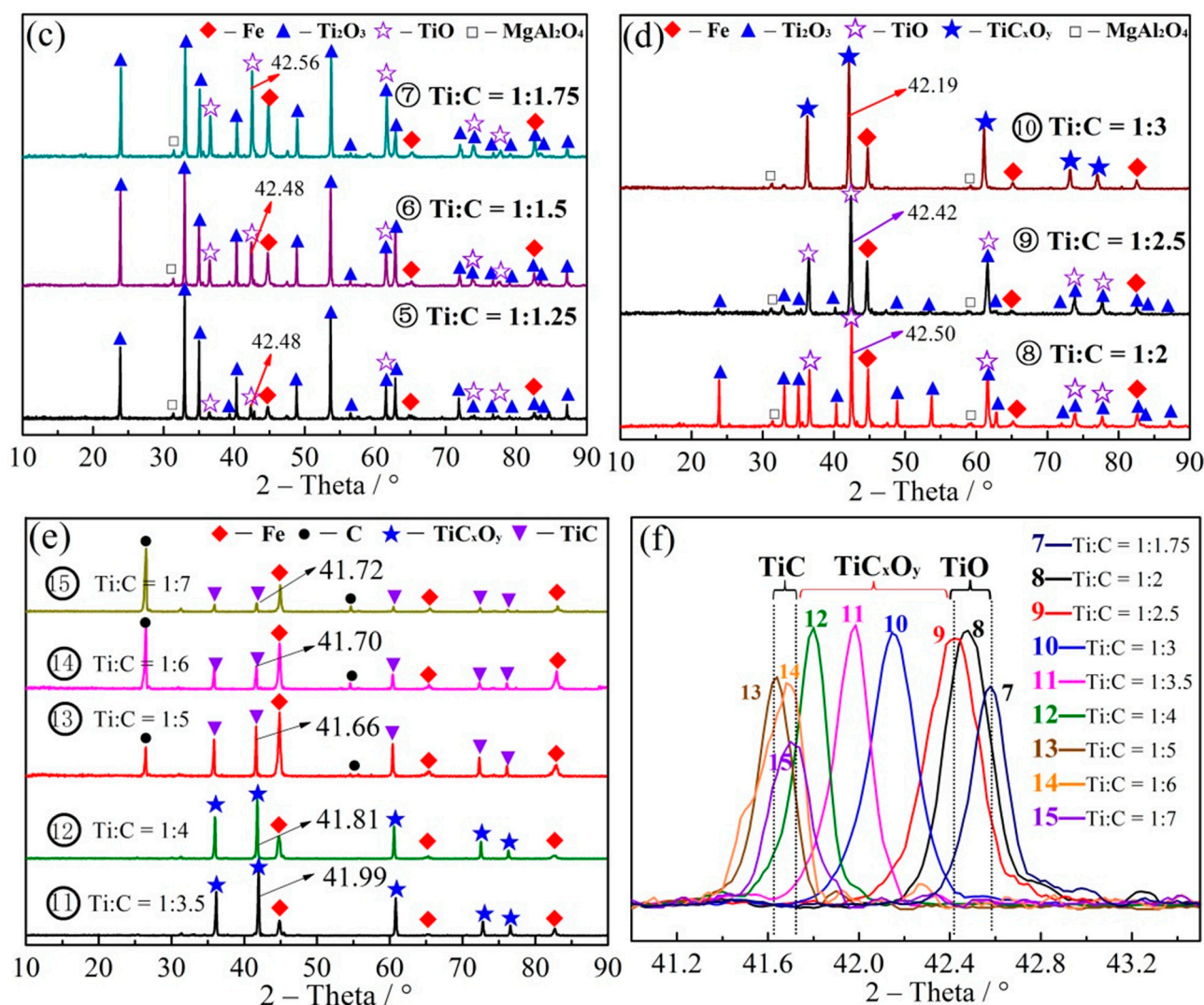


Figure 3. XRD patterns of the reduction products of (a) 1–2, (b) 3–4, (c) 5–7, and (d) 8–10, (e) 11–15; (f) XRD patterns with partial amplifications for the reduction products (7–15).

As shown in Figure 3a–e, FeTi_2O_5 is firstly reduced to FeTi_2O_5 and Fe under the condition of low carbon ratio (No. 1). After increasing the ratio of Ti:C to 1:0.5 (No. 2), new phase of Ti_2O_3 was appeared, indicating further reduction of FeTi_2O_5 to Ti_2O_3 . When Ti:C was developed to 1:0.75 (No. 3), the characteristic peak of FeTi_2O_5 was disappeared. Then, all FeTi_2O_5 was transformed into Ti_2O_3 and Fe as well as the appearance of TiO. As the ratio of carbon was continued to increase (No. 4), Ti_2O_3 was continually reduced to TiO, and the characteristic peak of TiO was enhanced in the XRD pattern. As carbon was further increased (No. 5–9), the characteristic peak of Ti_2O_3 was decreased and TiO characteristic peak at 42° was inclined, confirming that Ti_2O_3 has been gradually transformed to TiO with the appearance of characteristic peaks in the 2θ range of 42.48 – 42.56° . When the Ti:C ratio was 1:3, the characteristic peak at the 2θ of 42.42° moved slightly to 42.19° , indicating that a new object phase of TiC_xO_y has been appeared [33,34,48,49]. Figure 3e shows that the 2θ values of the reduction product was continuously decreased with the growth of carbon content, proving that carbon has been increased and oxygen is decreased in TiC_xO_y , until the Ti:C ratio of 1:5 and appearance of the characteristic peak of carbon at the 2θ of 26° . After that, the peak at 41.7° was stable and TiC_xO_y was completely reduced to TiC.

From Figure 3f, it can be seen that the characteristic peak position of the reduction products of samples No. 7–9 is similar to the characteristic peaks of TiO (at the 2θ range of 42.56 – 42.19°), while those of samples No. 13–15 were due to TiC at the 2θ range of

41.76–41.66°. Moreover, observation of peaks in the 2θ range of 42.42 and 41.7° for the reduction product of samples No. 10 to 12 indicated the TiC_xO_y phase. Normally, the greater 2θ , the larger oxygen content in TiC_xO_y . TiC_xO_y , with the enhanced carbon content, was gradually reduced by increasing the carbon ratio.

According to the amount of carbon, the order of products in carbothermal reduction reaction was $\text{FeTiO}_3 \rightarrow \text{FeTi}_2\text{O}_5 \rightarrow \text{Ti}_2\text{O}_3 + \text{Fe} \rightarrow \text{TiO} + \text{Fe} \rightarrow \text{TiC}_x\text{O}_y + \text{Fe} \rightarrow \text{TiC} + \text{Fe}$. The results here, however, show a difference from references [27,32–34]. The result of Gao et al. [27] show that the reduction sequence of FeTiO_3 was $\text{FeTiO}_3 \rightarrow \text{Ti}_n\text{O}_{2n-1} + \text{Fe} \rightarrow \text{Ti}_2\text{O}_3 + \text{Fe} \rightarrow \text{TiC}_x\text{O}_y + \text{Fe} \rightarrow \text{TiC} + \text{Fe}$. TiO did not appear. The result of Gou et al. [33,34] is similar with Gao, and TiO also did not appear. This may be due to that different experimental conditions, and also the reduction product was detected only by XRD, which would lead to misjudgment of phase. TiC is isomorphous with TiO and TiC_xO_y [50]. Therefore, to further clarify the phase of the reduction product and determine the reliability of TiO, TiC and TiC_xO_y in the reduction product, Ti 2p binding energy was measured.

3.1.2. XPS Analysis of the Reduction Products

It is well-known that TiC is isomorphous with TiO [50] and titanium in both shows distinct chemical affinity towards oxygen and carbon. In order to further clarify the phase of the reduction product and determine the reliability of TiC_xO_y in the reduction product, Ti 2p binding energy of pure TiO, TiC and Ti_2O_3 reagents were independently measured. Then, TiC and TiO were mixed in a 1:1 mole ratio and changes of the Ti 2p binding energy in the mixtures were monitored before and after sintering at 1550 °C for 4 h. Ti 2p binding energies of the reduction product of samples No.8–14 were, then, analyzed to determine the characteristics of TiC_xO_y . The optimal carbon ratio for the preparation of TiC_xO_y was clearly obtained via comparison with the Ti 2p of the pure reagents.

(1) XPS Spectra of Pure Reagents

Figure 4a,b shows the XPS spectra of Ti 2p for TiO and Ti_2O_3 pure reagents. The XPS spectra of the reduction product of sample No. 3 (Ti:C ratio of 1:0.75) are shown in Figure 4c.

As Figure 4a,b show, there are two distinct peaks that were precisely fitted to form two splitting doublets. The doublets located at 464.17–464.38 eV and 458.45–458.61 eV are typically attributed to Ti 2p_{1/2} and Ti 2p_{3/2} of Ti-O, respectively [50,51]. The Ti 2p peak positions of TiO and Ti_2O_3 were almost the same. Figure 4c depicts that the Ti 2p peak of Ti_2O_3 in the reduction product was the same as for pure Ti_2O_3 , indicating that Ti_2O_3 obtained by the reduction process is comparable to pure Ti_2O_3 reagent. Ti 2p peaks of pure TiO and TiC are also displayed in Figure 5a. Figure 5b shows the Ti 2p peaks in a mixture of TiC and TiO (1:1 mole ratio) before and after sintering at 1550 °C for 4 h. As shown in Figure 5a, Ti 2p peaks of TiC and TiO have different characteristic peak-positions. The peaks positioned at 455.25 and 458.48 eV are typically attributed to Ti 2p_{3/2} of TiC and TiO, respectively. Whereas, the peaks located at 461.12 and 464.17 eV are attributed to Ti 2p_{1/2} of TiC and TiO, respectively [50,52–55]. Therefore, the Ti 2p peaks can be used to distinguish TiO and TiC.

As can be seen from Figure 5b, Ti 2p_{3/2} and Ti 2p_{1/2} of the mixture of TiC and TiO (1:1 mole ratio) are different before and after sintering, such that the peak of Ti 2p before sintering is low on the left and high on the right; whereas this peak was high on the left and low on the right after 4 h sintering, confirming that TiC_xO_y solid solution would be formed after sintering. Therefore, according to the shape of Ti 2p_{3/2} and Ti 2p_{1/2} combined with the result of XRD, it can be judged whether the reduction product is TiO, TiC_xO_y or TiC. Subsequently, Ti 2p peaks can be utilized to determine the characteristics of TiO and TiC.

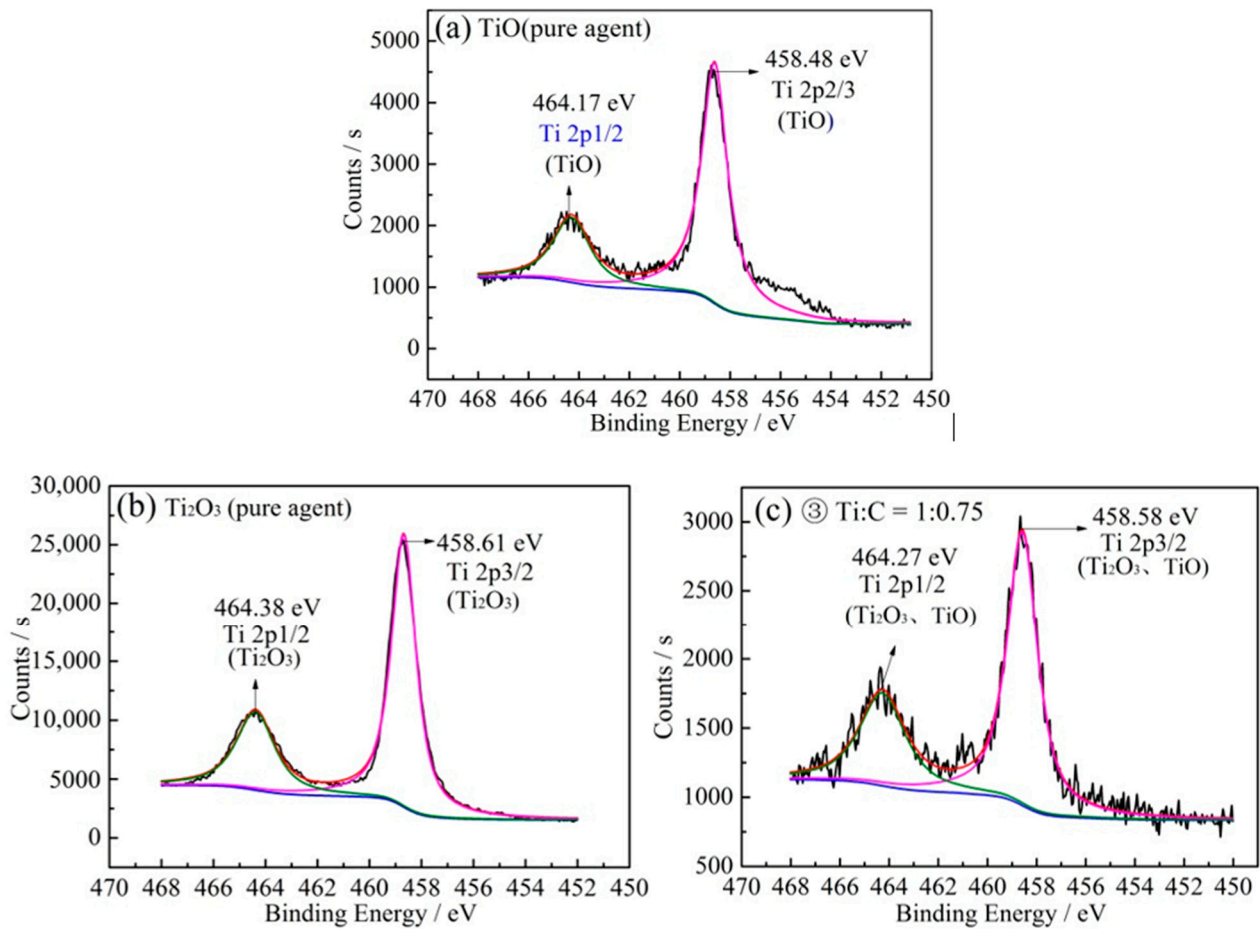


Figure 4. The Ti 2p_{2/3} and Ti 2p_{1/2} spectra of (a) TiO, (b) Ti₂O₃ and (c) reduction product with Ti:C, 1:0.75.

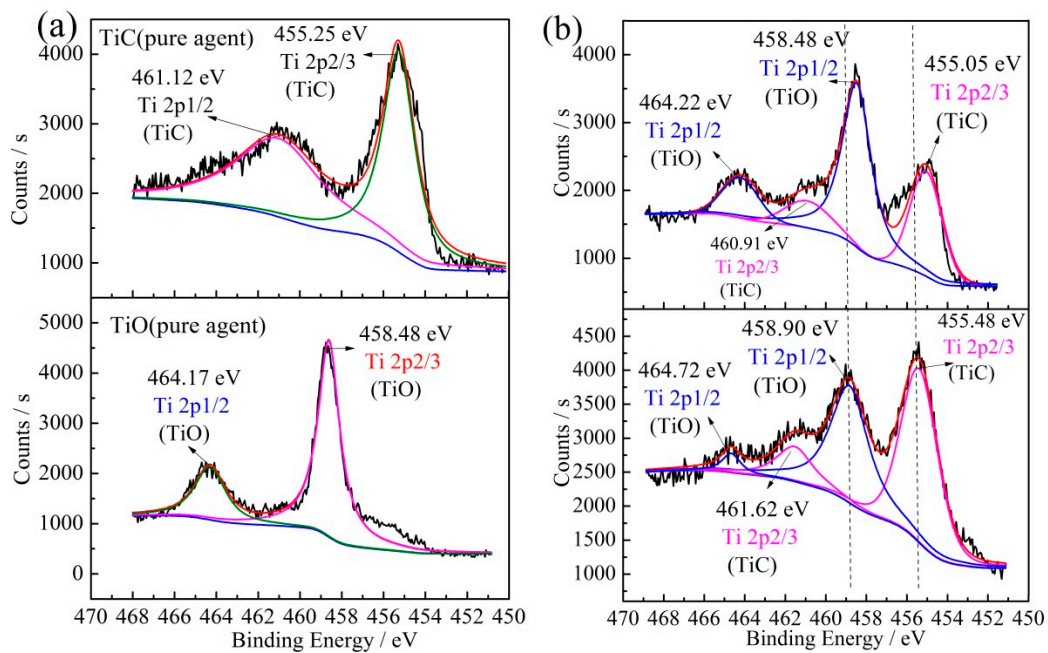


Figure 5. (a) Ti 2P spectra of pure TiO and TiC reagents, (b) Ti 2P spectra of a mixture of TiO and TiC (molar ratio of 1:1) before and after sintering (1550 °C under argon for 4 h sintering).

(2) XPS Spectra of the Reduction Products of Samples No. 9–14

The Ti 2P spectra of the reduction products of samples No. 9–14 are shown in Figure 6a–f, respectively. If the phase in No. 9 be judged only from the XRD characteristic peak at the 2θ value of 42.42° , then the main phases would be Fe, Ti_2O_3 and TiO. However, from analysis of Ti 2P in Figure 6a, it can be envisaged that the Ti 2p_{3/2} of TiC also appears at 455.43 eV (Ti-C), indicating that TiC_xO_y would be the reduction product when Ti:C is 1:2.5. The shape of Ti 2P spectra in Figure 6b–d is similar to that in Figure 5b, and Ti 2p_{3/2} peak of TiC has been obviously appeared at 455.06, 455.20 and 455.30 eV, indicating that TiC_xO_y is the main reduction product of samples 10–12. When Ti:C ratio is 1:3, 1:3.5 and 1:4, the reduction product is TiC_xO_y and Fe. The shape of Ti 2P spectra in Figure 6e,f is similar to that of pure TiC reagent and Ti 2p_{3/2} peak of TiC is prominent. When Ti:C ratio is 1:5 and 1:6, all titanium content is reduced to TiC.

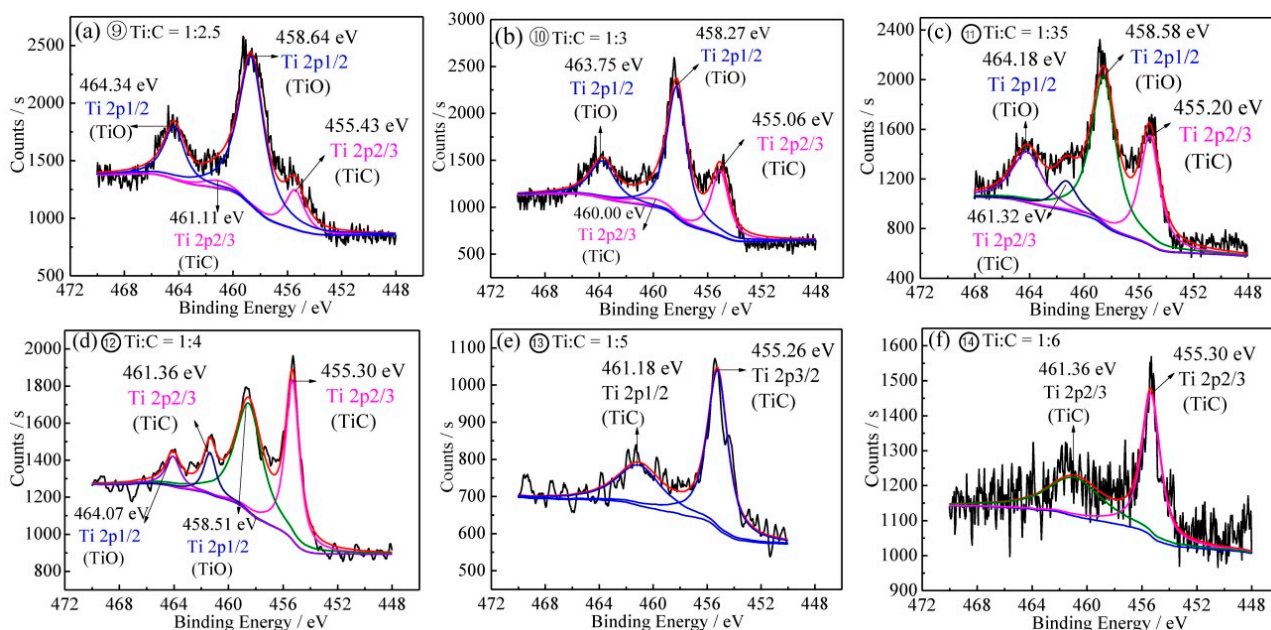


Figure 6. Ti 2P binding energy spectra (a–f) of the reduction product of samples 9–14 with different carbon contents.

In conclusion, XPS results for Ti 2p combined with XRD outputs confirmed that TiO, TiC and TiC_xO_y are the main products of carbon thermal reduction process. In practice, the ratio of Ti:C should be controlled in the range of 1:3–1:4 in the production of TiC_xO_y via carbothermal reduction of ilmenite at 1550°C .

3.2. Effects of Temperature and Time on the Carbothermal Reduction

Figure 7 shows effect of temperature on the carbothermal reduction at 1300, 1400, 1500, and 1550°C with the Ti:C ratio of 1:3 and the reduction holding time of 2 h. This Figure confirms that increasing the reduction temperature is helpful in the case of ilmenite. When the reduction temperature is 1400–1500 $^\circ\text{C}$, parts of Ti_2O_3 have not been reduced to TiC_xO_y , and the characteristic XRD peak of carbon is still obvious. However, carbon and Ti_2O_3 react completely at the reduction temperature of 1550°C and TiC_xO_y as well as Fe are the main produced phases of the reduction process. Figure 7b shows effect of the reduction time (0.5–4 h) on the carbothermal performance. Parts of Ti_2O_3 are still not reduced at the holding time of 0.5 and 1 h. However, Ti_2O_3 was reduced to TiC_xO_y after the holding time of 2 h. Carbon and CO diffuse to the surface of Ti_2O_3 by enhancing the reduction time and reduction of Ti_2O_3 will be improved.

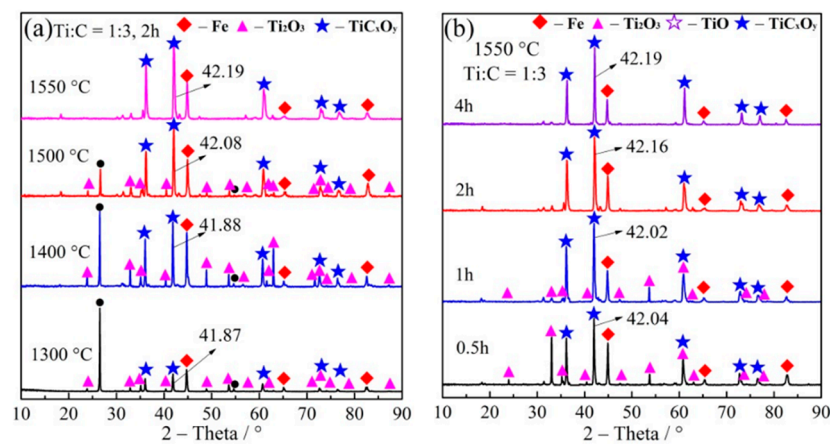


Figure 7. (a) XRD patterns of the reduction products of ilmenite at different temperatures; (b) XRD patterns of the reduction products of ilmenite at different times (1550 °C, Ti:C ratio of 1:3).

The scanning electron microscopy (SEM) and energy dispersive X-ray spectrometry (EDS) of the carbon thermal reduction products (No. 10, Ti:C of 1:3, reduction time of 4 h) are shown in Figure 8a,b.

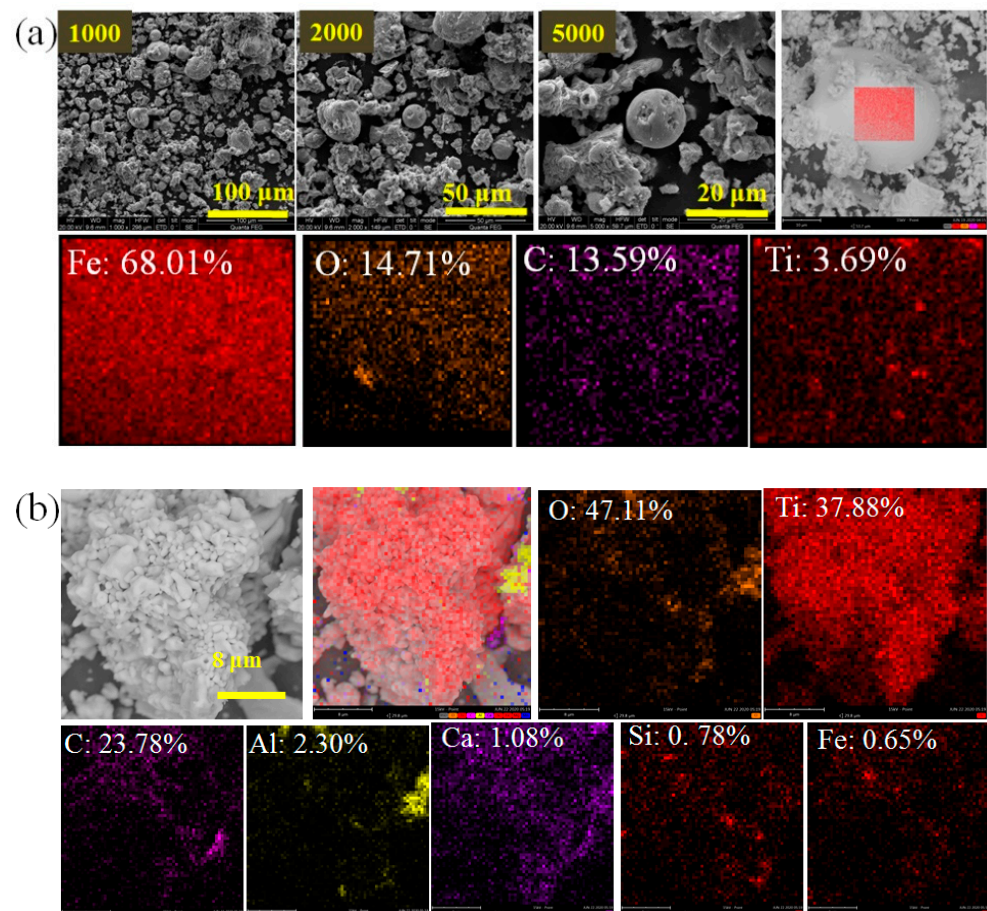


Figure 8. (a) SEM-EDS of the spherical shape reduction product; (b) SEM-EDS of the aggregated particles (EDS: atomic concentration). Scale bar (b): 8 μm.

The material with a spherical shape was attained, as shown in Figure 8a. Furthermore, the EDS results confirmed a spherical product composed of mostly metallic iron along with a small amount of Ti, C and O. In a high reduction temperature, iron was gathered to form

a droplet and grown up into a ball shape. As Figure 8b show, an aggregated morphology was achieved for the particles of the reduction product and the surface of particles is mainly Ti, C and O with a small amount of impurity elements of Fe, Mg, Ca, Mg, Al, Mg and Si. According to the atomic percentage and results of XRD and XPS, the main aggregated particles are TiC_xO_y .

3.3. Discussion on the Reduction Mechanism

According to the phase of the reduction product, possible reactions between graphite and ilmenite are depicted in Equations (1)–(12). In the case of solid carbon (C) as reductant, the possible reactions of ilmenite carbothermal reduction can be written as Equations (1)–(6). When CO used as the reducing agent, the carbothermal reduction reactions can be shown as Equations (7) and (8).

In order to understand the evolvement of carbon thermal reduction of ilmenite, the reaction mechanism was studied by consideration of the impact of temperature and Gibbs free energy (ΔG^θ) of the process via HSC Chemistry 6.0 software. The relationship between ΔG^θ and temperature (25–1600 °C) for the reactions of (1) to (12) is shown in Figure 9. Since there is no reported thermodynamic data on TiC_xO_y in HSC software, the ΔG^θ of TiC_xO_y cannot be obtained directly. The phase change in the reduction process is $TiO/Ti_2O_3 \rightarrow TiC_xO_y \rightarrow TiC$. Therefore, ΔG^θ of TiC_xO_y can be inferred from the reduction process of TiO or Ti_2O_3 .

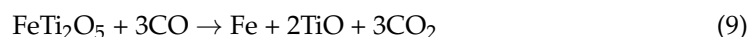
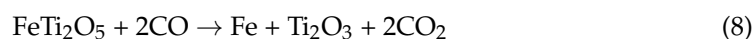
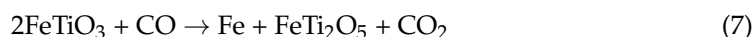
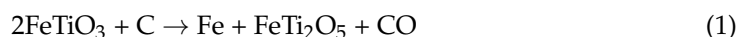


Figure 9a,b describe that ΔG^θ of Equations (1)–(9) become more negative as the temperature increases and the driving force of the reduction reaction was greatly enhanced with temperature. Equations (10)–(12) would not happen because of the positive ΔG^θ at the temperature range of 25 to 1600 °C. Therefore, TiO and Ti_2O_3 cannot be reduced to TiC by CO. Figure 9c shows that solid carbon, CO and CO_2 exist in reduction process and carbon can be converted to CO and CO_2 . Furthermore, diffusion of CO can improve the reduction process.

As shown in Figure 9a, when the temperature reached above 725, 775, and 925 °C, the ΔG^θ of Equations (1)–(3) was less than zero, thus, the reduction of $FeTiO_3$ and $FeTi_2O_5$ was favored and $FeTi_2O_5$, Ti_2O_3 and TiO were the chief products. When the temperature was higher than 1175 and 1325 °C, the ΔG^θ of Equations (5) and (6) was negative, therefore, TiO and Ti_2O_3 were reduced to TiC based on the amount of carbon. In the case of higher temperatures above 1600 °C, Ti_2O_3 can be reduced to TiO based on Equation (4). Although Equation (4) cannot perform at the reduction temperature of 1550 °C. Figure 9d shows that Ti_2O_3 has a stronger thermodynamic stability than TiO, therefore Ti_2O_3 cannot be reduced to TiO by carbon at this temperature.

As shown in Figure 9b, when the temperature is above 818 °C, the ΔG^θ of Equation (8) is less than zero and Equation (8) begins to accelerate the reduction of FeTi_2O_5 to produce Ti_2O_3 . In addition, at the temperatures above 1170 °C, ΔG^θ of Equation (7) is negative. However, the absolute value of ΔG^θ is very small and the reaction driving force may be small. When the temperature is higher than 1373 °C, the ΔG^θ of Equation (9) is less than zero and Equation (9) starts to accelerate the reduction of FeTi_2O_5 into Fe and TiO.

In conclusion, in the early and middle stages of carbothermal reduction of FeTiO_3 , solid carbon and CO participate in the reduction process and Ti_2O_3 content can be mainly affected by Equations (2), (6) and (8) with the increase of carbon ratio and TiO comes chiefly from Equations (3) and (9). When Ti:C is 1:2.5, Equations (3) and (9) are prominent for the production of TiO. By controlling the Ti:C ratio in the range of 1:3–1:4, the main reduction reaction in late stage is $\text{TiO}/\text{Ti}_2\text{O}_3 + \text{C} \rightarrow \text{TiC}_x\text{O}_y + \text{CO}$ and the ΔG^θ of TiC_xO_y is between TiC and TiO. In the late stage of the process, the reaction to generate TiC_xO_y or TiC is mainly caused by solid carbon. According to the amount of carbon, the order of products in carbothermal reduction reaction is $\text{FeTiO}_3 \rightarrow \text{FeTi}_2\text{O}_5 \rightarrow \text{Ti}_2\text{O}_3 + \text{Fe} \rightarrow \text{TiO} + \text{Fe} \rightarrow \text{TiC}_x\text{O}_y + \text{Fe} \rightarrow \text{TiC} + \text{Fe}$.

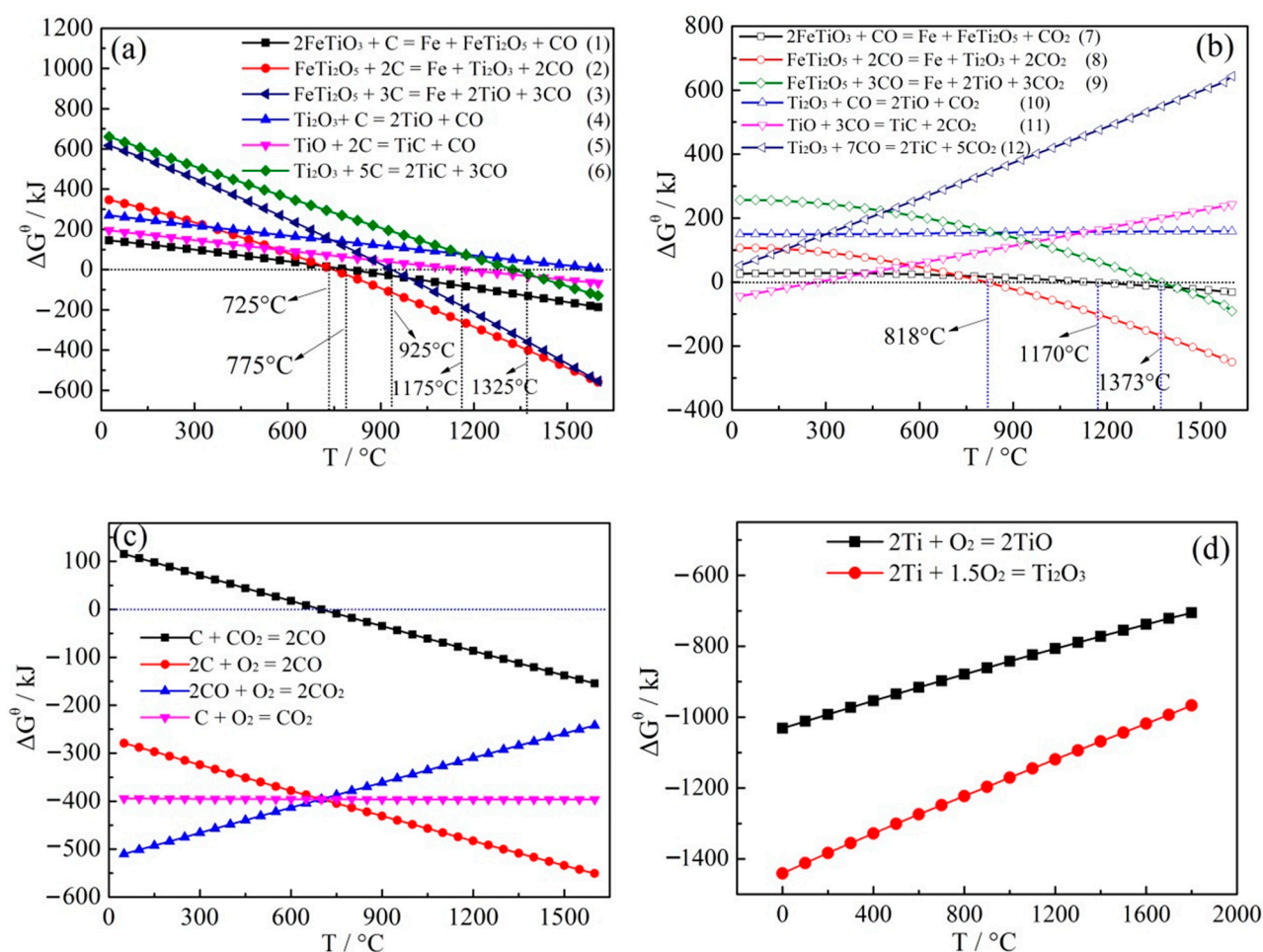


Figure 9. Correlation of ΔG^θ with temperature. (a) ΔG^θ - T for Equations (1)–(6); (b) ΔG^θ - T for Equations (7)–(12); (c) ΔG^θ - T for carbon system; (d) ΔG^θ - T for TiO and Ti_2O_3 .

3.4. Purification Experiments

3.4.1. Flotation and Magnetic Separation

300 g of the reduction products was obtained at 1550 °C with the Ti:C ratio of 1:3 and, then, was grinded by a ball mill for 60 min, screening as $-0.074 \mu\text{m} + 50 \mu\text{m}$, $-50 \mu\text{m} + 38 \mu\text{m}$ and $-38 \mu\text{m}$. Thereafter, kerosene flotation was carried out for decarburization

and magnetic separation of Fe. The product yields of flotation and magnetic separation are shown in Table 3. The XRD phase of product in each process is shown in Figure 10.

Table 3. Flotation and magnetic separation product yield under different particle sizes (%).

Product	Particle Size		
	−0.074 μm + 50 μm	−50 μm + 38 μm	−38 μm
Flotation Foam (Carbon-Bearing Part)	0	0	8.01
Flotation Tailings (TiC_xO_y , Fe)	100	100	91.99
Magnetic Separation (Non-Magnetic)	0.6	0	34.99
Magnetic Separation (Magnetism)	99.4	100	57

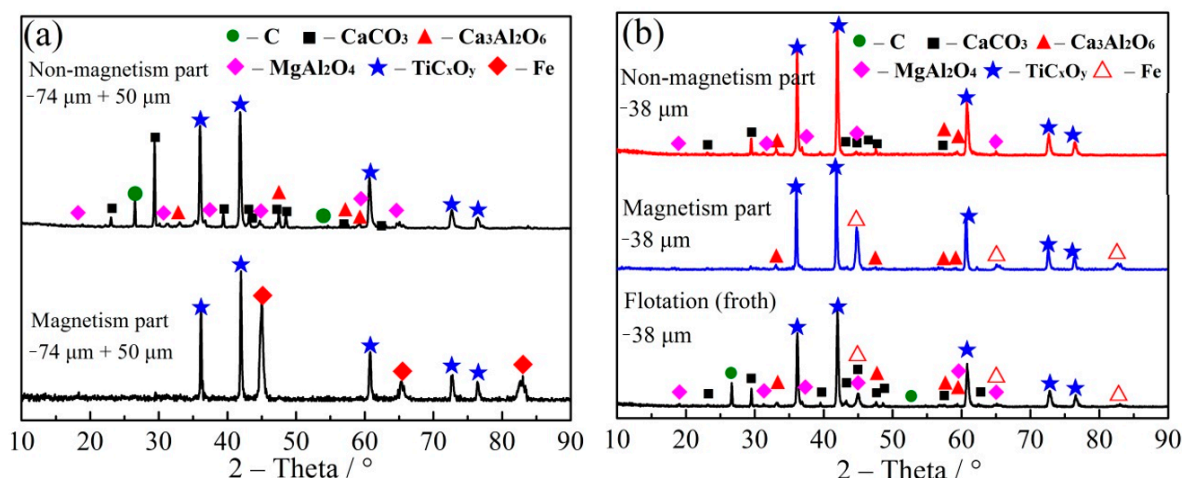


Figure 10. (a) XRD of magnetic separation product (particle size: $-50 \mu\text{m} + 38 \mu\text{m}$); (b) XRD patterns of the flotation product and the magnetic and the nonmagnetic parts (particle size: $-38 \mu\text{m}$).

It can be seen from Table 3 that the flotation yield of zero is attained with the particle size of $-0.074 \mu\text{m} + 50 \mu\text{m}$ and $-50 \mu\text{m} + 38 \mu\text{m}$. The yields of 99.4 and 100% were, respectively, attained for magnetic materials with the particle size of $-0.074 \mu\text{m} + 50 \mu\text{m}$ and $-50 \mu\text{m} + 38 \mu\text{m}$, respectively. In addition, the yields of 0.6 and 0% were gained for nonmagnetic materials, respectively. Figure 10a shows that the magnetic materials are TiC_xO_y and Fe. The yield of foam and nonmagnetic product was increased to 8 and 34.99%, respectively, after flotation and magnetic separation with the particle size of $-38 \mu\text{m}$. The flotation bubbles are C, CaCO_3 , MgAl_2O_4 , CaAl_2O_6 , Fe and TiC_xO_y (Figure 10b). Therefore, it can be concluded that TiC_xO_y , iron and residual carbon were not dissociated until the particle size of $-38 \mu\text{m}$. The nonmagnetic material contains TiC_xO_y , CaCO_3 , MgAl_2O_4 , CaAl_2O_6 and C. In a high temperature, calcium was combined with CO_2 to form CaCO_3 . In addition, magnesium, aluminum and calcium can be combined with oxygen to form MgAl_2O_4 and CaAl_2O_6 . After magnetic separation, iron was basically removed, and TiC_xO_y with less impurity was obtained. SEM-EDS (Figure 11) shows that Ca content is higher than other impurities in the sample.

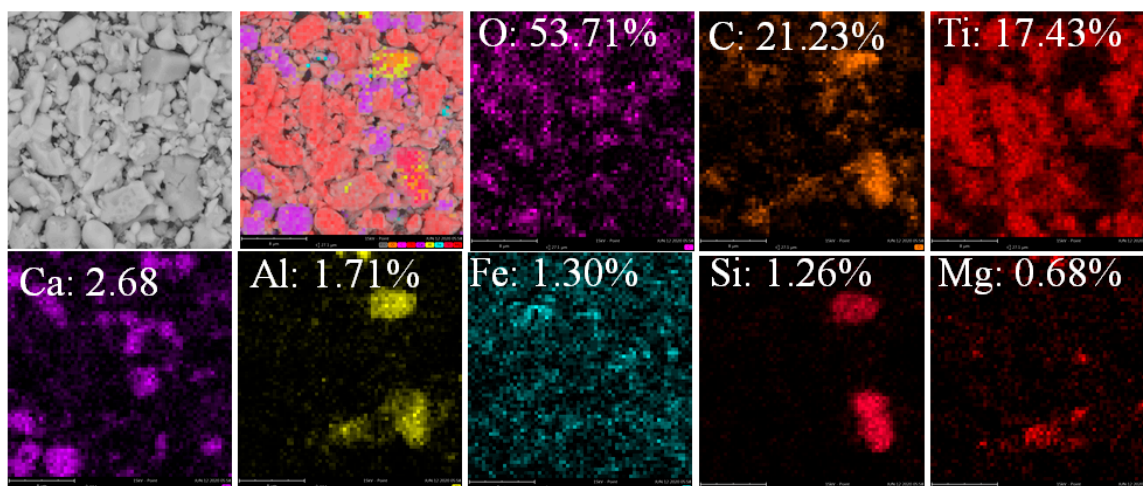


Figure 11. SEM-EDS of nonmagnetic part (EDS: atomic concentration). Scale bar: 8 μ m.

3.4.2. Acid Dissolution in Removing of Impurities

After flotation and magnetic separation, TiC_xO_y had still a little impurity of Fe , $CaCO_3$, $MgAl_2O_4$ and $CaAl_2O_6$. Especially, $CaCO_3$ and Fe were high in TiC_xO_y . Acid dissolution was performed in order to remove the impurities.

Effects of hydrochloric and nitric acids on the dissolution of impurities in TiC_xO_y are shown in Table 4. Moreover, the XRD pattern and SEM-EDS of products are also shown in Figure 12. The mass of TiC_xO_y was 1.5 g, the acid volume was 10 mL, the acid concentration was 2 mol/L, the temperature was 25 $^{\circ}C$, the acid dissolution reaction time was 2 h, and the stirring speed was fixed at 150 r/min.

Table 4. The content (wt %) of main elements before and after dissolution of impurities with different acids.

Element	Ca	Fe	Mg	Al	Si	Total Impurity
Before Acid Dissolution	5.03	3.65	1.05	1.90	0.75	12.37
Acid Dissolution: HNO_3	1.12	2.11	1.08	1.79	0.26	6.36
Acid Dissolution: HCl	1.05	0.27	1.16	1.77	0.32	4.56

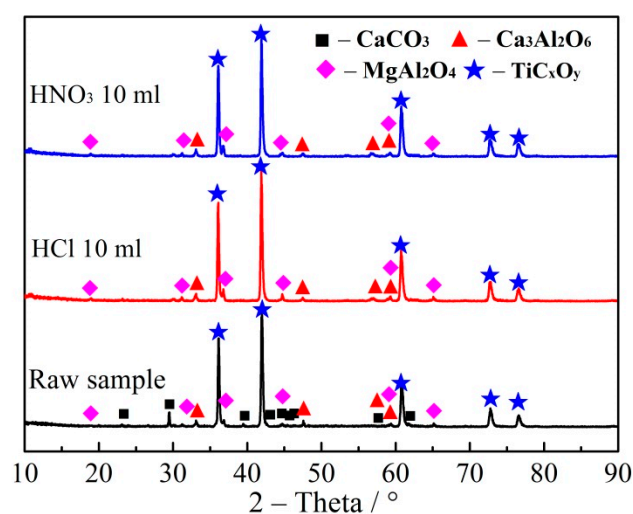


Figure 12. XRD patterns of products after removal of impurities by hydrochloric and nitric acids.

As shown in Table 4, the content of impurities in TiC_xO_y products before acid solution treatment was as high as 12.37%. Whereas, the content of impurity was reduced to 6.36 and 4.56% after treating with nitric acid and hydrochloric acid, respectively. The content of Ca and Fe impurity elements were decreased obviously after acid dissolution. Figure 12 shows that the characteristic peak of $CaCO_3$ has been disappeared, indicating that $CaCO_3$ in TiC_xO_y can be effectively removed by hydrochloric and nitric acid dissolution. The rest of Ca, Mg and Si in the form of $MgAl_2O_4$ and $Ca_3Al_2O_3$ were hardly removed by acid dissolution. But, the overall content of Mg, Al, Si, Ca and Fe impurities in the titanium dioxide products showed a downward trend after being washed with acid solution.

3.4.3. Removal of Fe by Iron-Bath

After magnetic separation, there are still a lot of TiC_xO_y and Fe in the magnetism part. In order to recovery of TiC_xO_y and Fe, a method of iron-bath was applied in a high temperature to remove Fe. Because of their different smelt point and density, TiC_xO_y would be floated on the liquid iron surface and iron would smelt in an iron-bath, therefore, can be separated from TiC_xO_y . The temperature of iron-bath was 1600 °C, and the time was 30 min under an argon atmosphere. After separation of Fe and the floated slag, the floated slag was grinded and purified by magnetic separation acid dissolution. Both of Fe and the floated slag were analyzed by XRD, as shown in Figure 13. TiC_xO_y and Fe were separated, and the floated slag was TiC_xO_y with a little impurity of Ca, Mg and Al. Resistance of TiC_xO_y is less than 0.05 Ω .

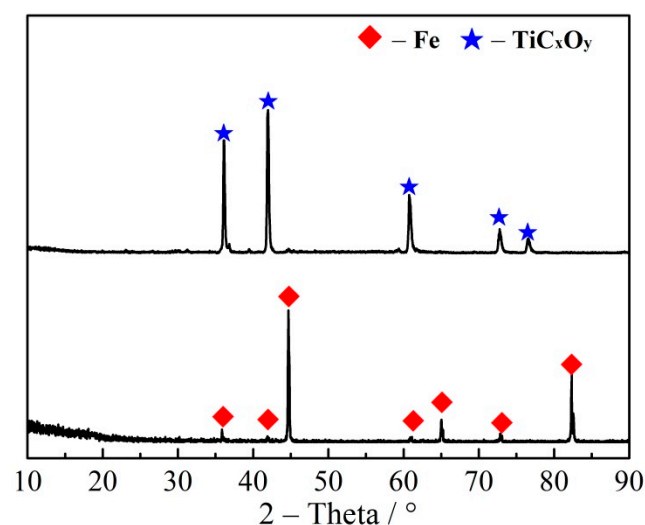


Figure 13. XRD patterns of iron and floated slag.

4. Conclusions

(1) Ilmenite ($FeTiO_3$) can be completely reduced to TiC_xO_y and Fe with the carbon content of 22.92–29.95% (Ti:C, 1:3–1:4) at 1550 °C and the reduction holding time of 2 h. Combining the XPS results of Ti with the phase analyses based on XRD experiments, the carbothermal reduction products TiO, TiC and TiC_xO_y can be thoroughly distinguished. At 1550 °C, the carbothermal reduction of ilmenite was gradually performed as $FeTiO_3 \rightarrow FeTi_2O_5 \rightarrow Ti_2O_3 + Fe \rightarrow TiO + Fe \rightarrow TiC_xO_y + Fe \rightarrow TiC + Fe$. The reaction thermodynamics and phase analysis show that the whole reduction process is principally involved the solid carbon and that the reduction capacity of CO is weak to produce TiC_xO_y . Due to the incomplete reduction state of TiC_xO_y , the ΔG^θ of TiC_xO_y is between TiC and TiO. In addition, the higher temperature leads to the shorter reduction time.

(2) Grinding, flotation and magnetic separation confirm that C, TiC_xO_y and Fe are not dissociated until the particle size of $-38 \mu m$. The $CaCO_3$ content in TiC_xO_y can be effectively removed by hydrochloric and nitric acid dissolution. TiC_xO_y and Fe can be

easily separated by an iron bath at a high temperature, and the float slag consists of TiC_xO_y together with a little impurity of Ca, Mg and Al. Resistance of TiC_xO_y is less than 0.05 Ω .

(3) In general, this research obtains the optimal conditions for the production of TiC_xO_y by carbothermal reduction from ilmenite, provides a beneficiation-metallurgy process for purification of reduction TiC_xO_y , and expands the application of ilmenite, provides basic parameters to reduce the cost of making titanium metal and improves the competitiveness of the existing enterprises.

Author Contributions: Methodology, C.H., W.D. and X.L.; writing—original draft preparation W.D. and C.H.; writing—review and editing, C.H. and C.Z.; investigation, C.Z. and J.Z.; conceptualization, S.M. and J.Y.; project administration, Y.W., T.F. and Z.W. All authors have read and agreed to the published version of the manuscript.

Funding: This research was funded by Science and Technology Major Project of Guangxi Province, grant number AA18118030, Natural Science Foundation Guangxi Province, grant number 2018GXNS-FAA281337, and the Natural Science Foundation of China, grant number NSFC 51804084, 51774099.

Institutional Review Board Statement: Not applicable.

Informed Consent Statement: Not applicable.

Data Availability Statement: The data presented in this study are available on request from the corresponding author. The data are not publicly available due to that this is also an enterprise industrialization project.

Acknowledgments: We want to acknowledge the support of Jin Mao Titanium Industry Company in Guangxi, China and Kaituo Wang for his advice.

Conflicts of Interest: The authors declare no conflict of interest. The funders had no role in the design of the study; in the collection, analyses, or interpretation of data; in the writing of the manuscript; or in the decision to publish the results.

References

1. Cui, C.X.; Hu, B.M.; Zhao, L.C.; Liu, S.J. Titanium alloy production technology, market prospects and industry development. *Mater. Des.* **2011**, *32*, 1684–1691. [[CrossRef](#)]
2. Sun, H.Y.; Wang, J.S.; Dong, X.J.; Xue, Q.G. A literature review of titanium slag metallurgical processes. *Metal. Int.* **2012**, *17*, 49–56.
3. Li, F.Q.; Mo, J.H.; Li, J.J.; Zhou, H.Y.; Huang, L. Study on the driver plate for electromagnetic forming of titanium alloy Ti-6Al-4V. *Int. J. Adv. Manuf. Technol.* **2013**, *69*, 127–137. [[CrossRef](#)]
4. Zhai, J.H.; Chen, P.; Wang, H.B.; Hu, Y.H.; Sun, W. Flotability improvement of ilmenite using attrition-scrubbing as a pretreatment method. *Minerals* **2017**, *7*, 13. [[CrossRef](#)]
5. Du, Y.S.; Meng, Q.Y.; Yuan, Z.T.; Ma, L.Q.; Xu, Y.K. Study on the flotation behavior and mechanism of ilmenite and titanite with sodium oleate. *Miner. Eng.* **2020**, *152*, 1–9. [[CrossRef](#)]
6. Mehdilo, A.; Irannajad, M.; Rezai, B. Effect of chemical composition and crystal chemistry on the zeta potential of ilmenite. *Colloids Surf. A Physicochem. Eng. Asp.* **2013**, *428*, 111–119. [[CrossRef](#)]
7. Boyer, R.R.; Briggs, R.D. The use of β titanium alloys in the aerospace industry. *J. Mater. Eng. Perform.* **2005**, *14*, 681–685. [[CrossRef](#)]
8. Ding, J.H.; Zhang, Y.; Li, L.X.; Li, H.M. Metallogenic geological characteristics and titanium resources potential in China. *Geol. China* **2020**, *47*, 627–644.
9. Kumar, J.; Khamba, J.S.; Mohapatra, S.K. Investigating and modeling tool-wear rate in the ultrasonic machining of titanium. *Int. J. Adv. Manuf. Technol.* **2009**, *41*, 1107–1117. [[CrossRef](#)]
10. Zhang, W.S.; Zhu, Z.W.; Cheng, C.Y. A literature review of titanium metallurgical processes. *Hydrometallurgy* **2011**, *108*, 177–188. [[CrossRef](#)]
11. Perks, C.; Mudd, G. Titanium, zirconium resources and production: A state of the art literature review. *Ore Geol. Rev.* **2019**, *107*, 629–646. [[CrossRef](#)]
12. EPoulsen, E.R.; Hall, J.A. Extractive Metallurgy of Titanium: A review of the state of the art and evolving production techniques. *JOM* **1983**, *35*, 60–65. [[CrossRef](#)]
13. Kroll, W.; Fink, C.G.; Summers, D.B. The production of ductile titanium. *Trans. Electrochem. Soc.* **1940**, *78*, 35–649. [[CrossRef](#)]
14. Hayes, F.H.; Bomberger, H.B.; Froes, F.H.; Kaufman, L.; Burte, H.M. Advances in titanium extraction metallurgy. *JOM* **1984**, *36*, 70–76. [[CrossRef](#)]
15. Chen, G.Z.; Fray, D.J.; Farthing, T.W. Direct electrochemical reduction of titanium dioxide to titanium in molten calcium chloride. *Nat. Cell Biol.* **2000**, *407*, 361–364. [[CrossRef](#)]

16. Fray, D.J. Emerging molten salt technologies for metals production. *JOM* **2001**, *53*, 27–31. [[CrossRef](#)]
17. Mohandas, K.S.; Fray, D.J. FFC cambridge process and removal of oxygen from metal-oxygen systems by molten salt electrolysis: An overview. *Trans. Indian Inst. Met.* **2004**, *57*, 579–592. Available online: <http://www.igcar.gov.in/transiim/2004/vol57-6overview.pdf> (accessed on 21 January 2021).
18. Fray, D.J.; Farthing, T.W.; Chen, Z. Removal of Oxygen from Metal Oxides and Solid Solutions by Electrolysis in a Fused Salt. Australian Patent WO9964638, 1999. Available online: https://www.lens.org/images/patent/AU/4277099/B2/20030403/AU_758931_B2.pdf (accessed on 21 January 2021).
19. Ono, K.; Suzuki, R.O. A new concept for producing ti sponge: Calciothermic reduction. *JOM* **2002**, *54*, 59–61. [[CrossRef](#)]
20. Gordo, E.; Chen, G.Z.; Fray, D.J. Toward optimisation of electrolytic reduction of solid chromium oxide to chromium powder in molten chloride salts. *Electrochim. Acta* **2004**, *49*, 2195–2208. [[CrossRef](#)]
21. Okabe, T.H.; Waseda, Y. Producing titanium through an electronically mediated reaction. *JOM* **1997**, *49*, 28–32. [[CrossRef](#)]
22. Okabe, T.H.; Oda, T.; Mitsuda, Y. Titanium powder production by preform reduction process (PRP). *J. Alloys Compd.* **2004**, *364*, 156–163. [[CrossRef](#)]
23. Zhu, H.M.; Jiao, S.Q.; Gu, X.F. Method for Producing Pure Titanium by Electrolysis of Titanium Monoxide/Titanium Carbide Soluble Solid Solution Anode. China Patent 200510011684, 2005. Available online: <https://www.zhangqiaokeyan.com/patent-detail/06120426166.html> (accessed on 21 January 2021).
24. Jiao, S.; Zhu, H. Electrolysis of Ti_2CO solid solution prepared by TiC and TiO_2 . *J. Alloys Compd.* **2007**, *438*, 243–246. [[CrossRef](#)]
25. Jiao, S.; Zhu, H. Novel metallurgical process for titanium production. *J. Mater. Res.* **2006**, *21*, 2172–2175. [[CrossRef](#)]
26. Wang, Q.; Song, J.; Wu, J.; Jiao, S.; Hou, J.; Zhu, H. A new consumable anode material of titanium oxycarbonitride for the USTB titanium process. *Phys. Chem. Chem. Phys.* **2014**, *16*, 8086–8091. [[CrossRef](#)] [[PubMed](#)]
27. Gao, C.; Jiang, B.; Cao, Z.; Huang, K.; Zhu, H. Preparation of titanium oxycarbide from various titanium raw materials: Part I. Carbothermal reduction. *Rare Met.* **2010**, *29*, 547–551. [[CrossRef](#)]
28. Jiang, B.; Xiao, J.; Huang, K.; Hou, J.; Jiao, S.; Zhu, H. Experimental and first-principles study of Ti-C-O system: Interplay of thermodynamic and structural properties. *J. Am. Ceram. Soc.* **2017**, *100*, 2253–2265. [[CrossRef](#)]
29. Cao, Z.; Xie, W.; Jung, I.-H.; Du, G.; Qiao, Z. Critical evaluation and thermodynamic optimization of the Ti-C-O system and its applications to carbothermic TiO_2 reduction process. *Met. Mater. Trans. A* **2015**, *46*, 1782–1801. [[CrossRef](#)]
30. Lefort, P.; Maître, A.; Tristant, P. Influence of the grain size on the reactivity of TiO_2/C mixtures. *J. Alloys Compd.* **2000**, *302*, 287–298. [[CrossRef](#)]
31. Dewan, M.A.; Zhang, G.; Ostrovski, O. Carbothermal reduction of titania in different gas atmospheres. *Met. Mater. Trans. A* **2008**, *40*, 62–69. [[CrossRef](#)]
32. Dewan, M.A.R.; Zhang, G.; Ostrovski, O. Carbothermal reduction of ilmenite concentrates and synthetic rutile in different gas atmospheres. *Miner. Process. Extr. Met.* **2011**, *120*, 111–117. [[CrossRef](#)]
33. Gou, H.-P.; Zhang, G.-H.; Chou, K.-C. Phase evolution during the carbothermic reduction process of ilmenite concentrate. *Met. Mater. Trans. A* **2014**, *46*, 48–56. [[CrossRef](#)]
34. Gou, H.-P.; Zhang, G.-H.; Hu, X.-J.; Chou, K.-C. Kinetic study on carbothermic reduction of ilmenite with activated carbon. *Trans. Nonferrous Met. Soc. China* **2017**, *27*, 1856–1861. [[CrossRef](#)]
35. Woo, Y.-C.; Kang, H.-J.; Kim, D.J. Formation of TiC particle during carbothermal reduction of TiO_2 . *J. Eur. Ceram. Soc.* **2007**, *27*, 719–722. [[CrossRef](#)]
36. Xiao, J.; Jiang, B.; Huang, K.; Jiao, S.; Zhu, H. Selective reduction of TiO_2-SiO_2 in the carbothermal reduction of titanium raw materials for preparation of titanium oxycarbide. In Proceedings of the 7th International Symposium on High-Temperature Metallurgical Processing, DOWNTOWN Nashville, TN, USA, 14–18 February 2016; Springer: Berlin/Heidelberg, Germany, 2016; pp. 419–425. [[CrossRef](#)]
37. Chen, X.; Deng, J.; Yu, R.; Chen, J.; Hu, P.; Xing, X. A simple oxidation route to prepare pseudobrookite from Panzhihua raw ilmenite. *J. Am. Ceram. Soc.* **2010**, *93*, 2968–2971. [[CrossRef](#)]
38. Nayak, D.; Ray, N.; Dash, N.; Rath, S.S.; Pati, S.; De, P.S. Induration aspects of low-grade ilmenite pellets: Optimization of oxidation parameters and characterization for direct reduction application. *Powder Technol.* **2021**, *380*, 408–420. [[CrossRef](#)]
39. Mojisola, T.; Ramakokovhu, M.; Raethel, J.; Olubambi, P.; Matizamhuka, W. In-situ processing and characterization of Fe-TiCN composite produced via enhanced carbonitrothermic reduction of low grade ilmenite concentrate. *Mater. Today Commun.* **2019**, *20*, 1–7. [[CrossRef](#)]
40. Lv, W.; Bai, C.; Lv, X.; Hu, K.; Lv, X.; Xiang, J.-Y.; Song, B. Carbothermic reduction of ilmenite concentrate in semi-molten state by adding sodium sulfate. *Powder Technol.* **2018**, *340*, 354–361. [[CrossRef](#)]
41. Lv, X.; Lv, X.; Xiang, J.-Y.; Wang, J.; Lv, X.; Bai, C.; Song, B. Effect of pre-oxidation on the carbothermic reduction of ilmenite concentrate powder. *Int. J. Miner. Process.* **2017**, *169*, 176–184. [[CrossRef](#)]
42. Lv, X.; Huang, R.; Wu, Q.; Xu, B.; Zhang, J. Non-isothermal reduction kinetics during vacuum carbothermal reduction of ilmenite concentrate. *Vacuum* **2019**, *160*, 139–145. [[CrossRef](#)]
43. Zhang, G.; Gou, H.; Wu, K.; Chou, K. Carbothermic reduction of panzhihua ilmenite in vacuum. *Vacuum* **2017**, *143*, 199–208. [[CrossRef](#)]
44. Gupta, A.K.; Aula, M.; Negre, E.; Viljanen, J.; Pauna, H.; Mäkelä, P.; Toivonen, J.; Huttula, M.; Fabritius, T. Analysis of ilmenite slag using laser-induced breakdown spectroscopy. *Minerals* **2020**, *10*, 855. [[CrossRef](#)]

45. Lv, W.; Lv, X.; Xiang, J.-Y.; Hu, K.; Zhao, S.; Dang, J.; Han, K.; Song, B. Effect of preoxidation on the reduction of ilmenite concentrate powder by hydrogen. *Int. J. Hydrogen Energy* **2019**, *44*, 4031–4040. [[CrossRef](#)]
46. Yuan, S.; Zhou, W.; Han, Y.; Li, Y. Efficient enrichment of low-grade refractory rhodochrosite by preconcentration-neutral suspension roasting-magnetic separation process. *Powder Technol.* **2020**, *361*, 529–539. [[CrossRef](#)]
47. He, C.L. Study on Microwave Absorption Characteristics of Typical Metallurgical Raw Material and Its Application. Ph.D. Thesis, Guangxi University, Nanning, China, 2016.
48. Gao, K.; Wang, Z.; Jia, Q.; Zhang, B.; Zhang, J. The utilization of carbon dioxide to prepare TiC_xO_y films with low friction and high anti-corrosion properties. *Coatings* **2020**, *10*, 533. [[CrossRef](#)]
49. Shanyan, H. Preparation of Titanium Oxycarbide TiC_xO_y and Its Structure Reseach. Ph.D. Thesis, University of Science & Technology Beijing, Beijing, China, 2010.
50. Oghenevweta, J.E.; Wexler, D.; Calka, A. Study of reaction sequences during MSR synthesis of TiC by controlled ball milling of titanium and graphite. *Mater. Charact.* **2018**, *140*, 299–311. [[CrossRef](#)]
51. Zhao, Z.; Diemant, T.; Rosenthal, D.; Christmann, K.; Bansmann, J.; Rauscher, H.; Behm, R.J. Au/TiO₂/Ru(0001) model catalysts and their interaction with CO. *Surf. Sci.* **2006**, *600*, 4992–5003. [[CrossRef](#)]
52. Xin, Z.; Lei, M.; Jian-Gang, W.; Hui-Min, Z. Investigation on ultrathin titanium oxide films synthesized by surface sol-gel method. *Optik* **2016**, *127*, 2780–2783. [[CrossRef](#)]
53. Felten, A.; Suarez-Martinez, I.; Ke, X.; Van Tendeloo, G.; Ghijsen, J.; Pireaux, J.-J.; Drube, W.; Bittencourt, C.; Ewels, C.P. The role of oxygen at the interface between titanium and carbon nanotubes. *ChemPhysChem* **2009**, *10*, 1799–1804. [[CrossRef](#)]
54. Li, G.; Xia, L. Structural characterization of TiC_x films prepared by plasma based ion implantation. *Thin Solid Film.* **2001**, *396*, 16–22. [[CrossRef](#)]
55. Parra, E.R.; Jose, P.; Arango, A.; Benavides, V.J. XPS Structure Analysis of TiN/TiC Bilayers Produced by Pulsed Vacuum Arc discharge. *Dyna* **2010**, *163*, 64–74. Available online: <https://www.researchgate.net/publication/49598678> (accessed on 21 January 2021).